Proceedings Paper:

Shi, Y. and Wang, J. orcid.org/0000-0003-4870-3744 (2019) Continuous demagnetization assessment for triple redundant 9-phase fault-tolerant permanent magnet machine. In: The Journal of Engineering. The 9th International Conference on Power Electronics, Machines and Drives, 17-19 Apr 2018, Liverpool, United Kingdom. Institution of Engineering and Technology (IET) .

https://doi.org/10.1049/joe.2018.8177

The Journal of Engineering

The 9th International Conference on Power Electronics, Machines and Drives (PEMD 2018)

Continuous demagnetisation assessment for triple redundant nine-phase fault-tolerant permanent magnet machine

eISSN 2051-3305
Received on 26th June 2018
Accepted on 30th July 2018
doi: 10.1049/joe.2018.8177
www.ietdl.org

Yanwen Shi[1], *Jiabin Wang*[1] ✉
[1]*Department of Electronic and Electrical Engineering, University of Sheffield, UK*
✉ *E-mail: j.b.wang@sheffield.ac.uk*

Abstract: In this study, the risk of partial irreversible demagnetisation of a triple redundant, nine-phase fault tolerant machine based on permanent-magnet-assisted synchronous reluctance machine topology has been comprehensively assessed under various faults, including the worst case scenario when the applied voltage vector is in the opposite direction of the back electromotive force due to sensing and inverter control failure, by employing a continuous demagnetisation model. The dynamic response during fault transients and the post-demagnetisation performance, such as the demagnetisation distribution, reduction in the back EMF and torque, will also be analysed and compared.

1 Introduction

Permanent-magnet-assisted synchronous reluctance machine (PMASynRM) has been an attractive option in automotive and safety critical applications because of its wide flux-weakening region, high torque density and efficiency as well as improved fault-tolerant capability. For permanent magnet (PM) machines, demagnetisation of magnets poses a particular safety risk because it can severely reduce the EMF and output torque, and increase the acoustic noise and vibrations. Since machines used in safety critical applications require high reliability, it is essential to accurately assess the risk of irreversible demagnetisation under various fault conditions.

It is well known that magnets are more vulnerable to large *d*-axis current. Investigations have been made to identify the worst fault condition which may produce the most significant demagnetising current and cause severe demagnetisation. It has been shown in [1] and [2] that the transient short-circuit current under the peak torque operation is much larger than that under the rated torque or peak power. In addition, it is reported in [1] and [2] that voltage reversal failure produces much higher demagnetising current than any short-circuit faults. Voltage reversal condition occurs when the voltage vector has incorrect 180 electrical degree offset with reference to the back EMF due to position sensor and/or controller failures.

Demagnetisation assessment has been studied in many publications. An analytical technique is described in [3] for predicting the risk of partial demagnetisation in quasi-Halbach magnetised tubular PM machines equipped with a modular stator winding by superimposing the armature reaction fields in the magnets. A set of simple analytical demagnetisation models is established in [4] to estimate the reduction of the EMF in surface-mounted PM machine under overload conditions. However, analytical approach is less accurate than finite-element (FE)-based approach and not applicable to machines with complex rotor structure. 2D FE-based approach is employed in [5] to assess the influence of PM machine type and different winding configurations on the demagnetisation risks. 3D FE simulations is utilised in [6] to show that reduction in stack length and high magnetic saturation will lead to considerable increase of demagnetisation resistance and further decrease the demagnetisation risk. All these approaches ignore the direction of magnetisation in a magnet and only use the magnitude of flux density in the demagnetisation assessment. This problem is addressed in [7] by predicting transient flux density at six points inside a magnet in the direction of the original magnetisation with due account of magnetic saturation. The flux density of all nodes in each magnet is decomposed in [1] into two components parallel and perpendicular to the magnetising direction. Subsequently, the flux density along the magnetising direction is used to assess partial irreversible demagnetisation under various fault conditions by 2D transient finite element analysis (FEA) with better accuracy.

However, all the above assessments cannot evaluate the post-demagnetisation performances to give a clear insight of the severity of demagnetisation behaviour. The post-demagnetisation performances of PM machines with different rotor structures and winding configurations are evaluated in [8] by a combination of magnetic equivalent circuit model and FE simulations. However, this method utilises data extracted at the peak demagnetising instant and does not consider the continuous accumulation of demagnetisation, causing prediction errors in the post-demagnetisation performance, particularly in fractional slot concentrated winding machines. An efficient searching algorithm employing the recoil line to iteratively find and update the new worst operating point below the knee point is introduced in [9]. At the same time, it gives a linear model which combines the partial irreversible demagnetisation and the temperature effects. The post-demagnetisation performance is assessed in [2] by tracking the history of partial demagnetisation via 2D FEA method. The minimum flux density in each element and extent of partial demagnetisation of every magnet can be accurately assessed. It also evaluates post-demagnetisation performance, such as the reduction in back-EMF and output torque, under various fault conditions, especially the voltage reversal fault.

The basic aims of this paper are to assess the demagnetisation withstand capability for a triple redundant, nine-phase (3×3-phase) fault machine based on PMASynRM topology as introduced in [10]. The risk of partial irreversible demagnetisation under various critical faults will be comprehensively assessed by employing a continuous demagnetisation model described in [2]. Additionally, the dynamic response during fault transients and the post-demagnetisation performance, such as the demagnetisation distribution, reduction in back EMF and torque, will also be evaluated.

2 Demagnetisation assessment for nine-phase 36-slot six-pole PMASynRM

The schematic of a 40 kW, triple redundant, nine-phase (3×3-phase) fault-tolerant PMASynRM reported in [10] is shown in Fig. 1. It employs six-pole and 36-slot with distributed windings configured as three independent three-phase windings. Each three-phase winding (ABC, DEF and GHI) does not overlap with the

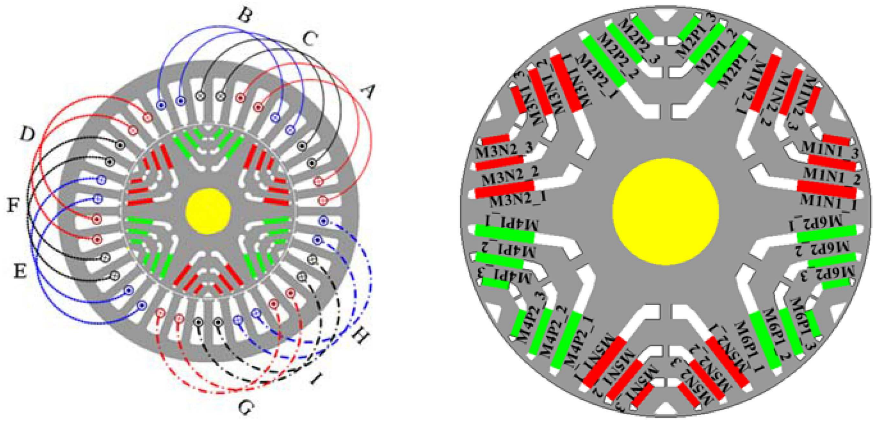

a *b*

Fig. 1 *Cross-section of nine-phase, 36-slot, six-pole PMASynRM*

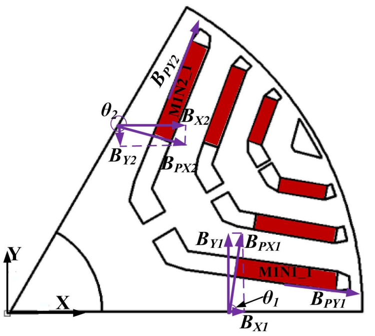

Fig. 2 *Decomposition of flux density of M1N1_1 and M1N2_1*

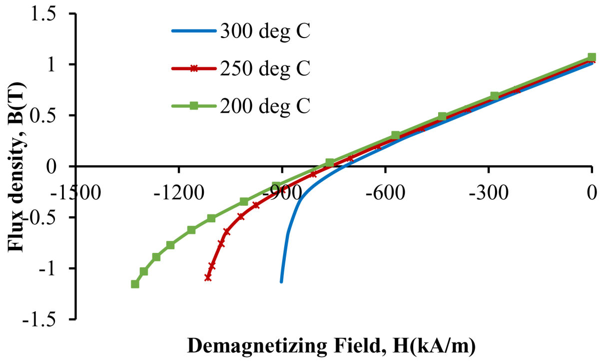

Fig. 3 *Demagnetization characteristics of VACOMAX 225 HR*

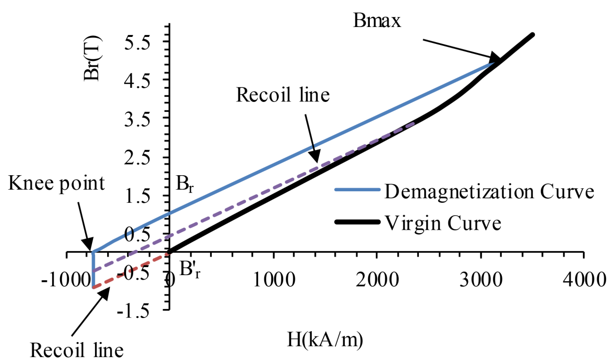

Fig. 4 *Demagnetization B–H curve with virgin curve at 300°C explaining partial demagnetization*

others and is controlled independently by a three-phase inverter in order to have physical, electrical and thermal isolations. The salient features of the machine are high reluctance torque and low PM field. This together with the triple redundancy makes the drive tolerant to most electrical faults. In Fig. 1, the magnets are shown in red and green as indicated by MiN/Pj_*k*, where $k = 1$, 2, 3 denotes the *k*th layer, $j = 1$, 2 denotes two different magnetisation angles of the *i*th rotor pole ($i = 1$–6), and *N* and *P* denote the polarity of magnetised direction.

The flux density in each magnet element is decomposed into two parts which are along and perpendicular to the magnetising direction [1]. Fig. 2 shows the schematic of flux density in one element of M1N1-1 and M1N2-1 along the magnetising direction

$$B_{PXn} = B_{Xn}\cos(\theta_n) + B_{Yn}\sin(\theta_n) \quad (1)$$

$$B_{PYn} = -B_{Xn}\sin(\theta_n) + B_{Yn}\cos(\theta_n) \quad (2)$$

where n is the element number; θ_n is the angle of magnetisation; B_{PXn} is the element flux density along the magnetising direction; B_{PYn} is the element flux density perpendicular to the magnetising direction. To prevent partial irreversible demagnetisation at a given element in a magnet, the flux density in the direction of magnetisation (B_{PXn}) must be larger than the value of the knee point.

The material of VACOMAX 225 HR is used for magnets in the machine. Fig. 3 shows the demagnetisation curves of the VACOMAX 225 HR for various operating temperatures. It is evident that the knee points for 200 and 250°C are around −0.5 T, while the knee point for 300°C is slightly lower than 0 T. In this study, the magnets are considered to be operated at 300°C and the knee point is set to be 0 T, viz., if the flux density in the direction of magnetisation goes below 0 T, partial irreversible demagnetisation will occur. Since the temperature coefficients of the magnets is very small and 300°C working temperature is exaggerated, the influence of temperature changing is not considered in the study.

Fig. 4 shows the demagnetisation *B*–*H* curve together with the virgin curve at 300°C for the continuous demagnetisation analysis described in [2]. It is based on continuous prediction of magnitude and direction of flux density in each element and uses the BH curve and recoil line of magnets and direction of the magnetisation to determine the remanence of magnets in each element in the next step. Thus, the magnet remanence in each element changes if the flux density in the direction of magnetisation is below its knee point. The process is implemented in 2D Opera, and can track the history of partial demagnetisation accurately. Hence, this method records the minimum flux density during the fault transient which can be used to assess partial demagnetisation. In addition, every first, second and third layer magnet are divided into 90, 78 and 42 elements, respectively. As every magnet element is calculated separately, different elements operate on different magnetisation levels. Therefore, it can evaluate post-demagnetisation performance, such as the demagnetisation distribution, and the reduction in back-EMF and output torque.

Fault conditions that are very critical with respect to partial irreversible demagnetisation considered in this paper are listed in Table 1. All of these faults are injected at the peak torque (114 N

Table 1 Fault conditions under consideration

	Fault	Pre-fault operation
*F*1	three-phase short-circuit	peak torque
*F*2	nine-phase short-circuit	peak torque
*F*3	turn-fault with three-phase terminal SC	peak torque
*F*4	turn-fault	peak torque
*F*5	three-phase voltage reversal	peak torque
*F*6	six-phase voltage reversal	peak torque
*F*7	nine-phase voltage reversal	peak torque

Table 2 Comparison of currents and post demagnetization performances under Faults *F*1 to *F*4

Fault	Peak phase current, A	Peak *d*-axis current, A	Steady-state short circuit current, A	Peak turn-fault current, A	% reduction in back EMF	% reduction in torque
*F*1	−233.60	−242	−85.43	—	0	0
*F*2	−218.77	−240	−85.43	—	0	0
*F*3	−140.82	−175	−85.43	−1664.45	0	0
*F*4	−146.70	−120	—	−1664.50	0	0

m) and base speed (4000 rpm). This operating condition has been shown to cause the most severer consequence than the rated torque or peak power operating conditions. *F*1 to *F*4 are various short-circuited fault conditions. *F*5, *F*6 and *F*7 consider voltage-reversal faults which are the worst scenarios because of much higher current than those in short-circuit conditions *F*1 to *F*4.

In 2D Opera, the switches are in parallel connection with the current sources and windings. The switches can be turned on at any rotor position to simulate a short circuit fault because it is verified in [1] that the instant of short circuit will not change the maximum demagnetising current. To simulate a voltage reversal fault, voltage sources are connected in parallel with the current sources, and both of them have separate switches for fault injection. Switches can be turned on without affecting each other when assessing the voltage reversal faults.

2.1 Demagnetisation assessment for short circuit faults

The performance indicators during transient process and after demagnetisation, including peak phase, *d*-axis, and turn-fault currents, steady-state short-circuit current, reduction in back EMF and output torque, of the PMASynRM under *F*1 to *F*4 have been compared in Table 2. The following observations can be obtained from the comparisons of the above four fault conditions at the peak torque and base speed.

i. Since no reduction in the back EMF and output torque are seen after the faults, *F*1, *F*2, *F*3 and *F*4 do not result in any degree of partial irreversible demagnetisation at the peak torque and base speed condition.
ii. Faults *F*3 and *F*4 generate huge circulating current in the faulted turn, however, because of the small inductance, the turn-fault current has little effect on the demagnetising flux. Hence, the turn-fault condition is less significant than the terminal short-circuit fault in respect of irreversible demagnetisation of this machine.

2.2 Demagnetisation assessment for voltage-reversal faults

The current trajectories in the *d*–*q*-axis plane and the output torque before and after Faults *F*5, *F*6 and *F*7 representing the three-phase, six-phase and nine-phase voltage-reversal faults are shown in Fig. 5. As observed in Figs. 5*a*, *c*, *e*, the trajectories begin at the pre-fault operation and pass the peak demagnetising currents identified by the arrows. The performance indicators during the transient process and after demagnetisation of the PMASynRM under *F*5 to *F*7 are shown in Table 3.

It can be observed from Fig. 5 and Table 3 that the peak transient current is an order of magnitude higher than the rated when the combined effect of the back-emf and full inverter voltage is only limited by the machine inductance under the voltage-reversal faults. It is also seen that the three-phase voltage-reversal condition generates the largest peak phase current (1366 A), while those of the six-phase and nine-phase voltage-reversals are slightly lower (1237 A). However, nine-phase voltage-reversal condition yields the highest peak *d*-axis current (1400 A) and the largest negative torque during transient process. Additionally, the back EMF and output torque after all three voltage-reversal faults have been reduced compared with the original value under healthy condition. This indicates that the magnets have suffered from significant partial irreversible demagnetisation under *F*5 to *F*7. Among all voltage-reversal faults, the three-phase voltage-reversal fault has the least irreversible demagnetisation while the nine-phase voltage reversal results in the most severe partial irreversible demagnetisation with 31.1% and 8.72% reductions in the back EMF and output torque, respectively.

However, even though the reductions in the back EMF under these faults are quite large, torque reduction only reaches 8.72% under the worst case. This is because the relatively small percentage (30%) of the alignment (PM) torque in the total output torque of the machine.

In order to evaluate the extent of the partial irreversible demagnetisation in every magnet, demagnetisation rate d_{mag} is introduced. It is defined by

$$d_{\text{mag}} = \frac{B_{\text{r}} - B'_{\text{r}}}{B_{\text{r}}} 100\% \tag{3}$$

where B_{r} is the pre-fault remanence and B_{r}' is the post-fault remanence of the permanent magnet of VACOMAX 225 HR at 300°C. According to this definition, d_{mag} will be zero if no irreversible demagnetisation takes place and increase with the severity of demagnetisation.

The demagnetisation rate of every magnet element under *F*5 to *F*7 is obtained and presented in Figs. 6*b*–*d*, respectively. Fig. 6*a* shows the corresponding position of all the magnets of the machine. The white area inside a magnet has no partial irreversible demagnetisation. It can be observed from Fig. 6*b* that the demagnetisation of the three-phase voltage-reversal condition is asymmetric and the worst demagnetised magnets which are marked with a red circle are M2P. As observed from Fig. 6*c*, the demagnetisation of six-phase voltage-reversal condition is also asymmetric, and the worst demagnetised magnets are marked with red circles which are M1N, M2P, M3N, M4P. It is also seen from Fig. 6*d* that the demagnetisation area of nine-phase voltage-reversal condition is almost symmetric. These figures also approve that the demagnetisation is worst under nine-phase voltage-reversal condition. Additionally, from the transient responses, it can be concluded that the most severe demagnetisation instant is when the negative *d*-axis current reaches the maximum value and the rotor

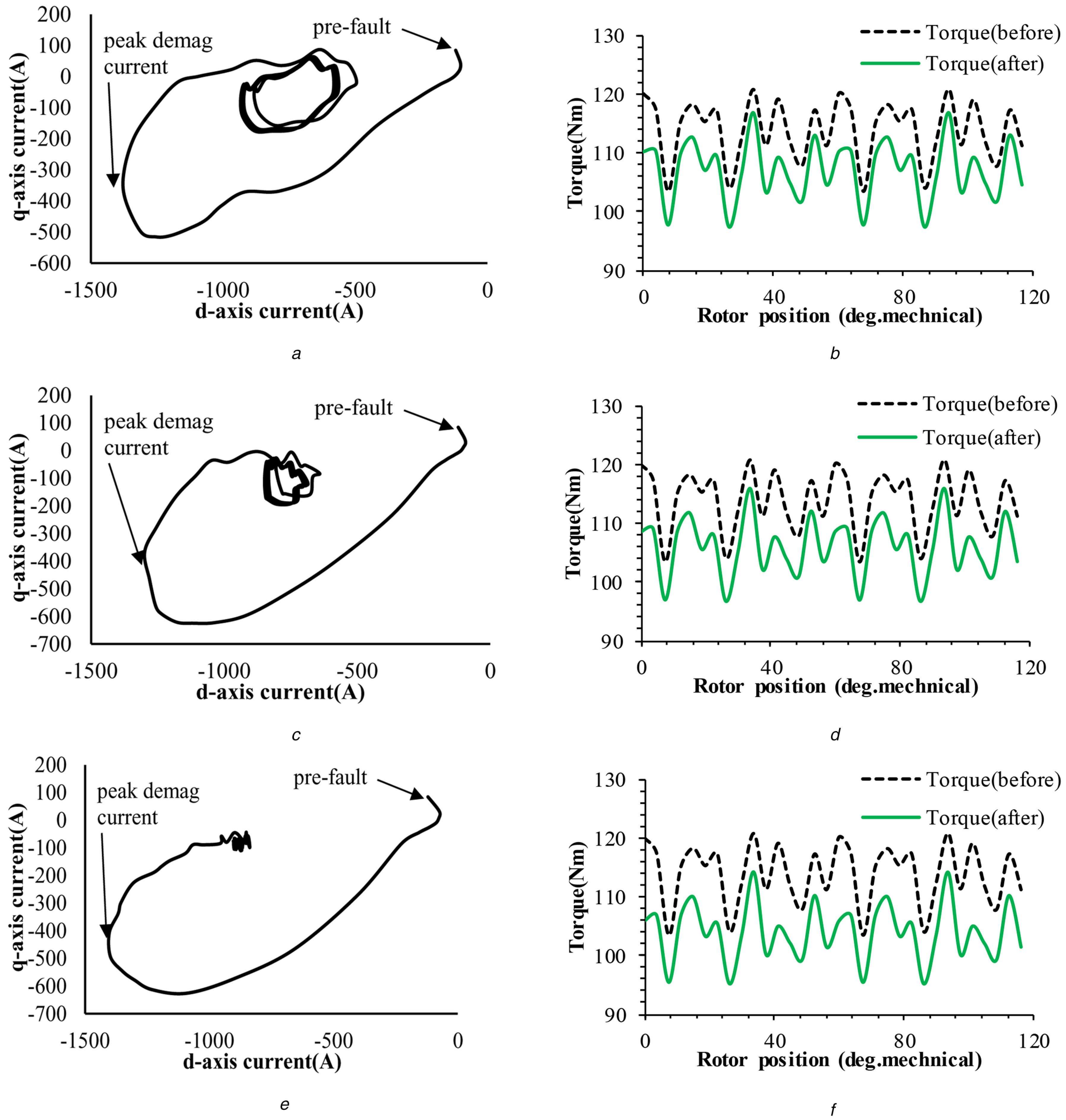

Fig. 5 *Current trajectories and output torque under various voltage-reversal conditions*
(a) *d*–*q*-axis current trajectory under *F*5, ***(b)*** Torque before and after *F*5, ***(c)*** *d*–*q*-axis current trajectory under *F*6, ***(d)*** Torque before and after *F*6, ***(e)*** *d*–*q*-axis current trajectory under *F*7, ***(f)*** Torque before and after *F*7

Table 3 Comparison of currents and post demagnetization performance under Faults *F*5 to *F7*

Fault	Peak phase current, A	Peak d-axis current, A	Corresponding *q*-axis current, A	Peak breaking torque, Nm	% Reduction in back EMF	% reduction in torque
*F*5	−1366	−1370	−392	3.74	20.91	5.93
*F*6	−1299	−1300	−367	−120	25.01	7.02
*F*7	−1237	−1400	−494	−282	31.34	8.72

magnets are aligned with the *d*-axis of the faulted windings at this instant.

Three- and six-phase voltage-reversal faults have generated asymmetric partial irrversible demagnetisation. Fig. 7 presents harmonic content of airgap flux density distribution in space over one pole-pair denoted by M1N and M2P before and after three-phase voltage-reversal fault. It can be observed that the second-order harmonic is present as a result of the asymmetric demagnetisation. However, because this machine employs integer-slot full-pitched distributed winding, the winding factor associated with even harmonics are zero. Thus, the additional even-space harmonics of the airgap flux density have no effect on the harmonic content of the back EMF. Additionally, with symmetric and balanced three-phase currents, no additional harmonics, especially second-order harmonic, will appear in the output torque after the asymmetric partial irreversible demagnetisation. This is indeed shown in Fig. 8. Hence, it follows that with integer-slot full-pitch distributed windings, the asymmetric demagnetisation will not result in additional harmonic frequencies in the output torque.

3 Summary

In this paper, the risk of partial irreversible demagnetisation for the triple redundant, fault-tolerant PMASynRM under various faults at the peak torque and base speed has been comprehensively assessed by employing a continuous demagnetisation model. Due to the advanced design features employed for the permanent magnet rotor, terminal and inter-turn short-circuit faults will not produce any degree of partial irreversible demagnetisation. However, all the voltage-reversal faults result in significant partial irreversible

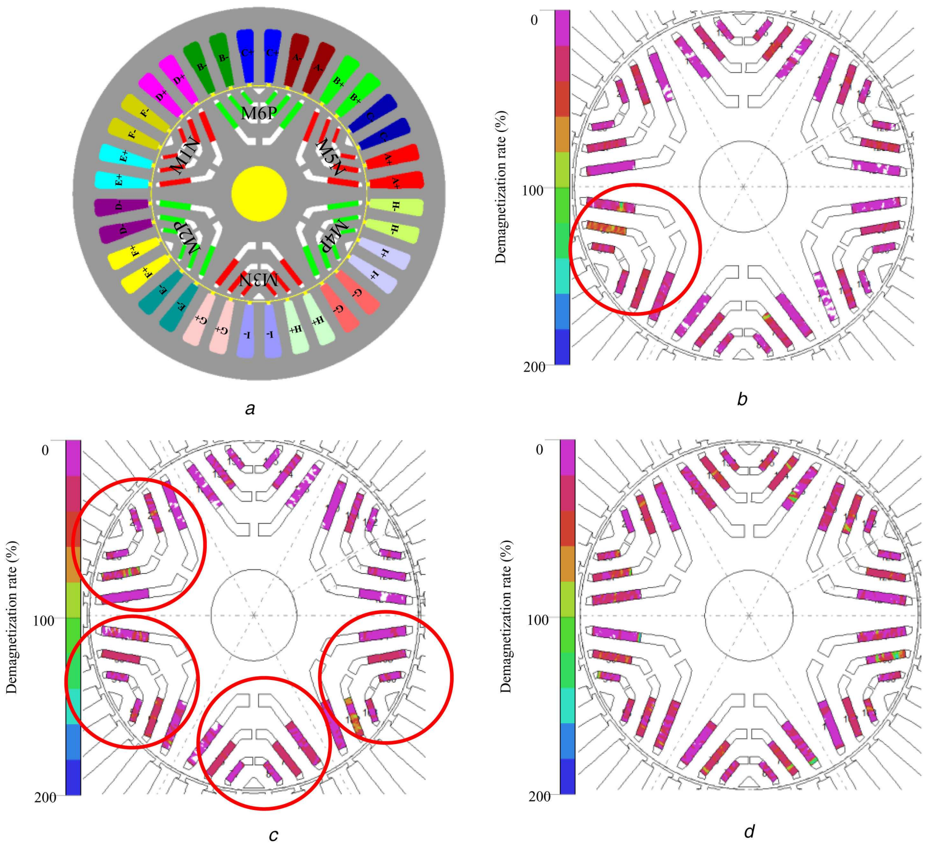

Fig. 6 *Partial demagnetised area after various voltage-reversal conditions*
(a) Original motor, ***(b)*** three-phase, ***(c)*** six-phase, ***(d)*** nine-phase

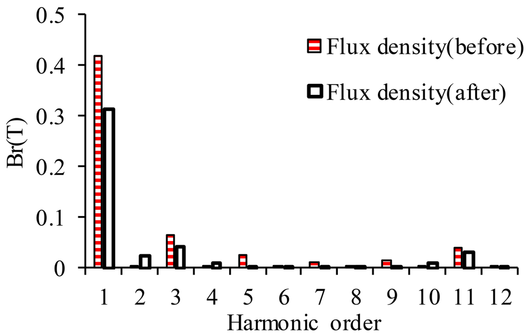

Fig. 7 *Space harmonic distribution of airgap flux density before and after F5*

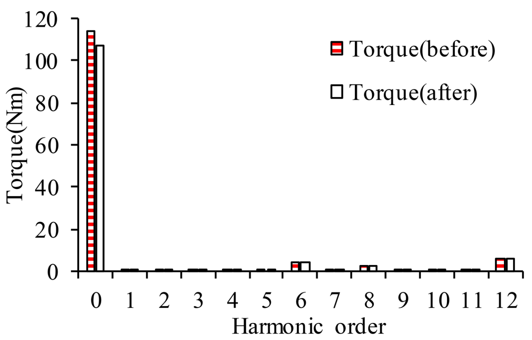

Fig. 8 *Torque harmonic distribution before and after F5*

demagnetisation. Among them, nine-phase voltage-reversal fault causes the symmetric and most severe partial irreversible demagnetisation and the resultant reduction in back EMF is 31.34%, but the reduction in output torque is only 8.72% which is modest. Further, the asymmetric demagnetisation will not lead to the additional harmonics in the output torque. The assessments demonstrate that the machine under study has very strong demagnetisation withstand capability.

4 References

[1] Patel, V.I., Wang, J., Nair, S.S.: 'Demagnetization assessment of fractional-slot and distributed wound 6-phase permanent magnet machines', *IEEE Trans. Magn.*, 2015, **51**, (6), pp. 1–11

[2] Nair, S.S., Patel, V.I., Wang, J.: 'Post-demagnetization performance assessment for interior permanent magnet AC machines', *IEEE Trans. Magn.*, 2016, **52**, (4), pp. 1–10

[3] Wang, J., Wang, W., Atallah, K., *et al.*: 'Demagnetization assessment for three-phase tubular brushless permanent-magnet machines', *IEEE Trans. Magn.*, 2008, **44**, (9), pp. 2195–2203

[4] Ruoho, S., Dlala, E., Arkkio, A.: 'Comparison of demagnetization models for finite-element analysis of permanent-magnet synchronous machines', *IEEE Trans. Magn.*, 2007, **43**, (11), pp. 3964–3968

[5] Choi, G., Jahns, T.: 'Demagnetization characteristics of permanent magnet synchronous machines'. IECON 2014-40th Annual Conf. of the IEEE Industrial Electronics Society, Dallas, TX, USA, 2014, pp. 469–475

[6] Kimiabeigi, M., Widmer, J., Baker, N., *et al.*: 'Three-dimensional modelling of demagnetization and utilization of poorer magnet materials for EV/HEV applications', *IEEE Trans. Energy Convers.*, 2016, **31**, (3), pp. 981–992

[7] McFarland, J.D., Jahns, T.M.: 'Investigation of the rotor demagnetization characteristics of interior PM synchronous machines during fault conditions', *IEEE Trans. Ind. Appl.*, 2014, **50**, pp. 2768–2775

[8] Choi, G., Jahns, T.M.: 'Post demagnetization characteristics of permanent magnet synchronous machines'. Energy Conversion Congress Exposition (ECCE), Montreal, Canada, 2015, pp. 1781–1788

[9] Zhou, P., Lin, D., Xiao, Y., *et al.*: 'Temperature-dependent demagnetization model of permanent magnets for finite element analysis', *IEEE Trans. Magn.*, 2012, **48**, pp. 1031–1034

[10] Wang, B., Wang, J., Griffo, A.: 'A fault tolerant machine drive based on permanent magnet assisted synchronous reluctance machine'. Energy Conversion Congress and Exposition (ECCE), Milwaukee, WI, USA, 2016